October 1981

Piezomodulation spectroscopy of molecular crystals. II. The pyromellitic dianhydride anthracene electron donor–acceptor complex

J. Merski
University of Nebraska - Lincoln

Craig J. Eckhardt
University of Nebraska - Lincoln, ceckhardt1@unl.edu

Piezomodulation spectroscopy of molecular crystals.[a] II. The pyromellitic dianhydride–anthracene electron donor–acceptor complex[b]

J. Merski[c] and C. J. Eckhardt[d]

Department of Chemistry, University of Nebraska, Lincoln, Nebraska 68588
(Received 9 October 1980; accepted 3 March 1981)

Piezomodulated reflection spectra are presented for the crystalline complex of pyromellitic dianhydride–anthracene. Two differently polarized charge transfer transitions are found and their strain sensitivities are obtained. The role of the charge transfer interaction in determining the magnitude of the piezomodulation is assessed. The piezomodulation spectra are found to have the response expected for an oriented gas. Significant enhancement of structure is also observed and is correlated with structure observed at 20 K.

I. INTRODUCTION

In the previous paper[1] the effects of piezomodulation on the spectra of a variety of crystal types were discussed. Two main categories are of interest: those crystals which behave as oriented gases (very weak coupling) and those which show significant coupling. Previous studies from this laboratory[2] have shown that, in many cases, electron donor–acceptor (EDA) complexes exhibit relatively weak exciton interactions.

The particular complex chosen for investigation here is that of pyromellitic dianhydride (PMDA) with anthracene (A). This complex has recently become the object of some attention. Haarer has reported the existence of a zero-phonon line in the 2 K PMDA–A crystal spectrum at the threshold of the lowest energy singlet charge transfer (CT) exciton transition. Subsequent high resolution, low temperature, single crystal spectra by the same group have also shown side bands associated with the zero-phonon line which are attributed to excitations of the fundamental vibrations of the complex.[3] Reflection spectra by Brillante and Philpott have shown structure on the CT band with intervals on the order of tens of wave numbers. Study of this system has led these investigators to conclude that the CT excitons are very weakly coupled.[4]

An early x-ray crystallographic structure was reported by Boeyens and Herbstein.[5] Recently, Robertson and Stezowski[6] have reported a high resolution structure at 153 K. The crystal is comprised of well defined mixed stacks of alternating donor (anthracene) and acceptor (PMDA) molecules. The relative dispositions of the moieties forming the complex with a given stack resemble that of adjacent layers in graphite.

The high resolution structure determination is in general agreement with the earlier work. However, the adjacent mixed stacks are found to form an interleaving network in which crystal packing forces are unusually large, thereby resulting in a considerable distortion of the anthracene and PMDA molecular conformations. Specifically, one end ring of anthracene is bent out of the mean plane formed by the other two. The anhydride portions of the PMDA molecule are also twisted out of the mean molecular plane. Consequently, the carbonyl oxygen atoms of a particular anhydride moiety of PMDA occupy substantially different crystallographic environments resulting in a measureable inequality of the two carbon–oxygen bond lengths.

Thus, the crystal structure and spectra of the crystal have been well studied although the spectra have only been obtained for the region of CT transitions. No study has been made of the intramolecular transitions.

Although anthracene is spectroscopically well characterized, the electronic structure of the PMDA molecule is uncertain. Ferstandig *et al.* were the first to thoroughly investigate 1 : 1 complex formation of PMDA with a large variety of polysubstituted benzene derivatives.[7] The reported molecular complex equilibrium constants and associated thermodynamic data obtained from analyses of solution spectra of the complexes via the Benesi–Hildebrand[8] method reveal the exceptionally strong acceptor properties of PMDA.

The nature of the EDA interaction had early suggested observation of the behavior of CT transitions under pressure. The effect of overlap of donor and acceptor orbitals on both the frequency and intensity of the CT transition has been studied in several laboratories at high pressure.[9,10]

The PMDA–A crystalline complex was selected as a model system for study by piezomodulation spectroscopy. In order to anticipate the effect of piezomodulation upon the CT band in particular, a phenomenological theory of pressure effects on CT transitions is recapitulated in the next section. The subsequent section gives experimental details and is followed by sections which present the spectra of the free complex and the crystal. The latter deals with both direct and piezomodulated determinations and presents analysis of the piezoreflection line shape for the determination of the strain-induced frequency shifts of the observed transitions. The

[a] Research supported by the Solid State Chemistry Program, Division of Materials Research of the National Science Foundation (DMR 79-08-759).
[b] Part I of the series is J. Merski and C. J. Eckhardt, J. Chem. Phys. 75, 3691 (1981).
[c] Part of a dissertation submitted to the University of Nebraska in partial requirement for the Ph. D. degree.
[d] John Simon Guggenheim Fellow, 1979–80.

 0021-9606/81/203705-14$01.00

presentation of the Kramers-Kronig transforms of the data follows and assignment of transitions are made based on the increased structural information. Finally, the results are compared with theory and the role of the piezomodulation is assessed.

II. THEORY

Offen and Nakashima[10] have formulated a phenomenological description of pressure effects on the charge transfer transition energy employing the equation $E_{CT} = h\nu_{CT} \cong \Delta + [(\beta_0^2 + \beta_1^2)/\Delta]$. The quantity Δ is equal to $W_1 - W_0$, where W_1 and W_0 are the energies of the dative and "no-bond" states, respectively.[11] Furthermore, W_{01} is the interaction energy between the "no-bond" and dative states which have an overlap of S_{01}. For an assumed proportionality between W_{01} and S_{01} of

$$W_{01} = kS_{01}, \quad \text{where } k \gg W_0 \text{ and } W_1 \ ,$$

β_0 and β_1 become

$$\beta_0 = (k - W_0)S_{01} = kS_{01} \approx \beta_1 \ .$$

Neglecting dispersion interactions,

$$E_{CT} = (W_1 - W_0) + \frac{2k^2 S_{01}^2}{(W_1 - W_0)} \ . \tag{2.1}$$

The pressure-induced shift of the charge transfer transition energy is

$$dE_{CT} = d(W_1 - W_0) + \left[\frac{2k^2 dS_{01}^2}{(W_1 - W_0)} - \frac{2k^2 S_{01}^2}{(W_1 - W_0)^2} d(W_1 - W_0)\right], \tag{2.2}$$

in which it is assumed that all shifts may be expressed as differentials. The two opposing contributions to dE_{CT} may be recognized by considering the composition of Δ. The differential change in Δ due to a compression of the complex is expected to shift E_{CT} to lower energy (red shift). This follows incontrovertibly, for weak complexes, from a consideration of the large attractive Coulomb interactions associated with the dative resonance structure $\psi_1(D^+-A^-)$, which makes a considerably larger contribution to the excited state than to the ground state. In addition to the red shift of E_{CT} due to Coulomb interactions of the $D^+ \cdots A^-$ type, a strain-induced change in the difference in van der Waals energies between ψ_0 and ψ_1 is expected to supplement the former.

The second term of Eq. (2.2) contributes a compressional blue shift to dE_{CT} which could potentially overwhelm, or greatly diminish, the red shift because the overlap integral S_{01} and its corresponding differential change are exponential functions of the donor–acceptor distance. At low pressures, however, the red shift contributions to dE_{CT} are expected to predominate.

A determination of dE_{CT} by absorption or reflection spectroscopy permits an evaluation of the difference in gradients of the excited and ground state molecular complex potentials corresponding to R_{DA}^N, the equilibrium acceptor–donor distance of the ground state, because the excitation is vertical. In fluorescence experiments, however, measurement of dE_{CT} allows one to deduce the difference in the gradients of the ground and excited state potentials corresponding to the excited state equilibrium donor–acceptor distance R_{DA}^E with Kasha's rule assumed. The foregoing neglects contributions to dE_{CT} due to strain-induced changes in donor–acceptor orientations and assumes that dE_{CT} is attributable to a single configuration coordinate change dR_{DA}.

The rigorous expression for the electronic charge transfer transition moment is

$$\mu_{CT} = e\langle \psi_E | \mathbf{r} | \psi_N \rangle \ . \tag{2.3}$$

Mulliken[12] approximates this by

$$\mu_{CT} \cong a^* b\, e(\mathbf{r}_D^m - \mathbf{r}_A^m) + (aa^* - bb^*)\, eS_{01}(\mathbf{r}_D^m - \mathbf{r}_{DA}^m) \ , \tag{2.4}$$

where $\mathbf{r}_D^m$ represents the mean position of an electron in a donor molecular orbital, $\mathbf{r}_A^m$ represents the corresponding vector for an acceptor orbital, and $\mathbf{r}_{DA}^m$ corresponds to the mean position of an electron characterized by a charge distribution determined by S_{01} (or the donor–acceptor orbital overlap S_{DA}). The vector $\mathbf{r}_{DA}^m$ may be expected, for planar donor and acceptor molecules, to terminate at some point along the normal to the mean molecular planes. Large deviations of μ_{CT} from the line of centers is not anticipated for weak complexes which are characterized by small values of S_{01}.

Both of the terms which contribute to μ_{CT} indicate that the intensity of the charge transfer transition is susceptible to strain modulation. Kadhim and Offen[13] have measured the pressure-induced intensity effects of the charge transfer absorption for a series of weak complexes.

III. EXPERIMENTAL

High quality single crystals of PMDA–A suitable for spectroscopic examination were obtained by solution growth procedures. Blue-violet fluorescence grade anthracene was used without further purification. Purification of PMDA was effected by means of successive vacuum sublimations. PMDA–A crystals were obtained by combining separately prepared solutions containing equimolar quantities of anthracene and PMDA dissolved in methyl ethyl ketone and allowing growth by evaporation.

The single crystal, high resolution x-ray structure determination[6] of PMDA–A at 153 K indicates that the crystals are triclinic with a space group symmetry of $P\bar{1}$ and $Z = 1$. By optical goniometry the following assignments for crystal faces zonal to the needle axis were obtained: $(\bar{1}10)$, (010), and (100), where (010) is the main face. Consistent with the above zonal face assignments are the (001) and $(00\bar{1})$ designations for the tip faces which intersect the needle or crystal c axis. The optically assigned indices were confirmed by x-ray crystallography.

The principal axes relevant to the (001) face exhibited minimal dispersion over the 15 000 to 40 000 cm^{-1} energy region. Consequently, reflection spectra for (001) were obtained for polarization directions coincident with either E or $E_\perp$ defined relative to the crystal morphology by Fig. 1.

Both the absence of symmetry constraints and the more complex in-plane dielectric susceptibility tensor

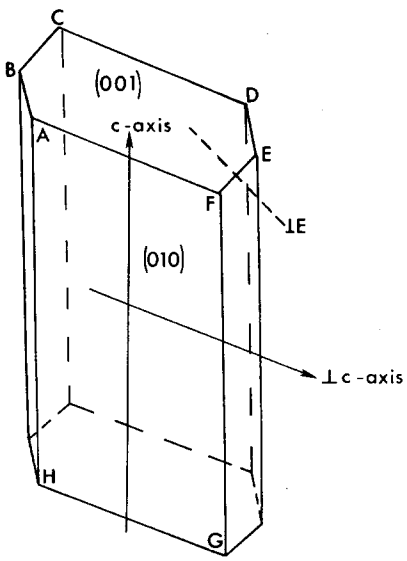

FIG. 1. PMDA–A crystal morphology.

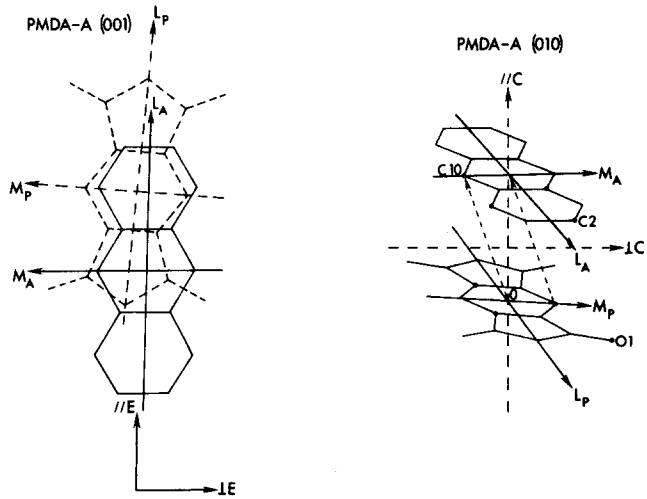

FIG. 3. Projection of PMDA–A onto the (010) and (001) faces.

result in significant (010) face axial dispersion. The experimentally measured dispersion is shown in Fig. 2. The 0° value for the ordinate corresponds to a coincidence between the polarization vector of the incident light and the crystal c axis (or $c_\perp$ axis for the second principal direction). Over the energy range from 15 000 to 20 000 cm^{-1}, reflection and piezoreflection spectra were obtained by maintaining a fixed incident light polarization and rotating the crystal to follow the angular dispersion. At 18 200 cm^{-1} the principal directions were found to coincide with c and $c_\perp$ within an experimental error of ± 2°. At energies greater than ≈ 25 000 cm^{-1}, axial dispersion was small and reasonably constant. The best average principal directions in this region correspond to a 15° clockwise rotation of c and $c_\perp$ shown in Fig. 1. Failure to follow this axial dispersion, particularly from 15 000 to 20 000 cm^{-1}, may be expected to affect the observed reflectivity line shape. This dispersion has not been reported in earlier studies. For convenience, the principal directions will be referred to as c and $c_\perp$.

The contents of the unit cell are shown projected onto the (010) and (001) crystal faces in Fig. 3. Conventional axial notation is used and is appropriately subscripted by A for anthracene and P for PMDA. The squared direction cosines between the molecular axes as well as the complex line of centers and the principal direction vectors are listed in Table I.

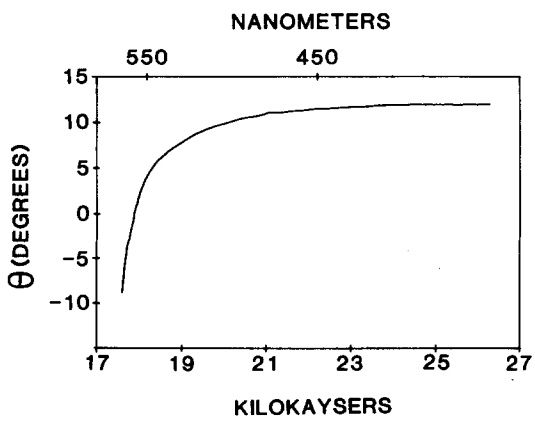

FIG. 2. PMDA–A axial dispersion for (010).

IV. FREE COMPLEX SPECTROSCOPY

The acquisition of solution spectroscopic data to obtain "free molecule" electronic or vibronic transitions is necessary for an understanding of crystal excitations. In lieu of the usually formidable *ab initio* calculations, an acceptable description of the latter may be realized by a parametrization of the crystal interaction calculations by well established free molecule spectroscopic quantities.

Spectroscopic data for anthracene are well known. The S_1 [(0, 0) transition] of anthracene which occurs at 26 700 cm^{-1} in iso-octane has been assigned as the short axis polarized $^1B_{2u} \leftarrow {}^1A_{1g}$ excitation. The absorption spectrum in the 25 000 to 36 000 cm^{-1} region consists of progressions and combinations derived from the a_g and b_{3g} molecular vibrations. Bree *et al.*[14] have determined that the most intense vibronic transitions are due to the excitation of vibrational modes with energies of (in cm^{-1}) 392, 1169, 1396, 1498, and 1462. The preponderance of anthracene vibrations in the 1100–1500 cm^{-1} range results in a low resolution absorption spectrum which appears to be comprised of five or six vibronic transitions based on a 1400 cm^{-1} progression. Adopting this simplified description of the S_1 vibronic transitions, one obtains from Craig[15] the following Franck–Condon factors ξ_u^2 for the first five members of the progression: 0.324, 0.316, 0.218, 0.092, and 0.050. We obtain the following transition energies in iso-octane (in cm^{-1}): 26 700, 28 250, 29 750, 31 230, and 32 600. Furthermore, Craig[15] reports an electronic dipole length of 0.61 Å.

The second singlet S_2 transition of anthracene occurs at 39 700 cm^{-1} in iso-octane and is assigned as the long axis polarized $^1B_{1u} \leftarrow {}^1A_{1g}$ excitation. The corresponding

TABLE I. Squared direction cosines between molecular axes and principal directions on (010) and (001).

Principal direction	Face	$\hat{L}_A$	$\hat{M}_A$	$\hat{N}_A$	$\hat{L}_P$	$\hat{M}_P$	$\hat{N}_P$	$\hat{c}^a$
$\parallel \hat{c}'$[b]	(010)	0.068	0.069	0.864	0.068	0.037	0.895	0.933
$\perp \hat{c}'$	(010)	0.169	0.811	0.019	0.111	0.875	0.009	0.067
$\parallel \hat{E}$	(001)	0.907	0.0001	0.093	0.892	0.006	0.102	0.391
$\perp \hat{E}$	(001)	0.0006	0.987	0.012	0.009	0.987	0.003	0.005

[a]PMDA–A complex center-to-center vector.
[b]Prime indicates an average principal direction in the 25 000 to 45 000 cm^{-1} region.

transition dipole length is 1.87 Å

Although an intensive investigation of the PMDA molecular electronic structure was considered beyond the scope or intent of the spectroscopic objectives associated with the study of the PMDA–A crystal system, knowledge of the spectral absorption profile of PMDA is necessary for the recognition of those excitations arising from the intermolecular charge transfer. Figure 4 displays the absorption spectrum of PMDA in glacial acetic acid in the 30 000–35 000 cm^{-1} energy region. The solution spectrum is insufficient to establish polarizations, but the relatively intense absorptions in the spectrum probably derive from excitations polarized in the mean molecular plane. This implicity assumes that the possible $\pi^* - n$ transitions polarized normal to the molecular plane possess insufficient intensity to produce the observed absorptions, since $\pi^* - n$ transitions are characterized by molar extinction coefficients of ~ 10–100.[16] The measured dipole strength of the PMDA absorption which spans the spectrum shown is 0.101 $Å^2$.

The CT absorption of PMDA–A in methyl ethyl ketone was obtained and analyzed according to standard procedures.[17] The peak absorption was observed at $\tilde{\nu}_{max}$ = 21 280 cm^{-1}. The PMDA and anthracene molecular absorptions in the 25 000–40 000 cm^{-1} region precluded the detection of higher energy charge transfer transitions.

The observed absorbance values for the CT band solution data were analyzed using least squares procedures after subtraction of the S_1 absorption of anthracene according to the Benesi–Hildebrand,[8] Foster–Hammick–Wardley,[18] and Scott[19] methods to obtain values for K_{eq} and the peak molar absorptivity. The latter and the corresponding average values obtained from the three methods of analysis are listed in Table II.

The values obtained and the absorption bandwidth at half-height were used to calculate, under the assumption of a Gaussian band profile, the charge transfer transition dipole strengths listed in Table II. The average dipole strength for the CT band is 0.143 $Å^2$.

V. CRYSTAL SPECTROSCOPY

A. Reflection spectra

The polarized, single crystal reflection spectra obtained from the (010) and (001) faces of PMDA–A are shown in Figs. 5 and 6. Excluding the rapid rise in crystal reflectivity at energies greater than 40 000 cm^{-1}, enhanced specular reflection occurs at 18 200, 20 000 (shoulder), and 33 200 cm^{-1} in the c spectrum of (010). The corresponding reflectivities for the above are 12.96%, 7.34%, and 5.85%, respectively. Weak structure is also seen at 24 200, ≈ 27 400, and 38 600 cm^{-1}. The c direction coincides with the center-to-center vector of the PMDA–A complex and is ~ 20° to the normal of the anthracene and PMDA molecular planes. Consequently, only a small amount of in-plane

TABLE II. Solution spectroscopy results.

Transition	$\tilde{\nu}_{max}$ (kK)	Method	a_{max} (ℓ/mol cm)	K_{eq}	d^2 ($Å^2$)
PMDA–A CT-I band	21.28	Benesi–Hildebrand	2.188×10^3	0.350	0.204
		Scott	1.074×10^3	0.727	0.100
		F–H–W	1.352×10^3	0.574	0.126
		Average	$1.538\times10^3 \pm 5.80\times10^2$	0.550 ± 0.190	0.143 ± 0.054
PMDA	31.75	Spectrum in glacial	2.396×10^3		0.101
	32.79	acetic acid	2.225×10^3		
	~34		$\sim 1.2\times10^3$		
Anthracene					
$\hat{M}_A$ ($^1B_{2u} \leftarrow {}^1A_{1g}$)	26.7	Spectrum in			0.372
$\hat{L}_A$ ($^1B_{1u} \leftarrow {}^1A_{1g}$)	39.7	iso-octane			3.50

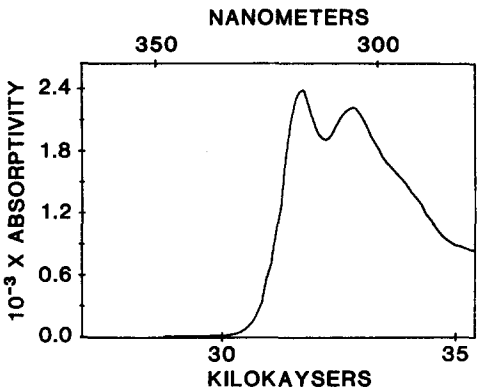

FIG. 4. PMDA absorption spectrum in glacial acetic acid.

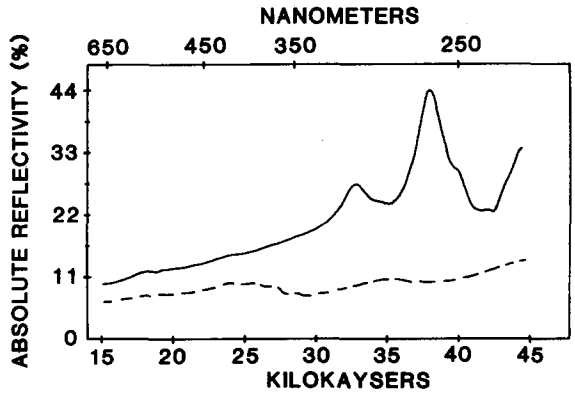

FIG. 6. PMDA–A reflection spectra at 300 K for the E-axis (—) and $\mathbf{E}_\perp$-axis (---) directions on (001).

intensity projects onto the c axis. The latter, together with the absence of intramolecular transitions in the ~ 15 000–25 000 cm^{-1} energy region, permits assignment of the lowest energy charge transfer transition CT-I which is responsible for the reflection band observed between 18 200 and 22 600 cm^{-1}. A comparison with the energy corresponding to the peak reflectivity of CT-I and the charge transfer transition energy observed in the solution spectrum indicates a – 3080 cm^{-1} crystal shift of the transition energy. This sizeable red shift of the CT-I transition energy is usually indicative of a strong crystal interaction.

Accompanying CT-I are, apparently, two higher energy charge transfer transitions CT-II and CT-III which produce weak reflection structure at 24 200 and ≈ 27 400 cm^{-1}, respectively. This structure, although invariably present in the reflection spectra, could be well resolved only by the application of piezoreflection techniques.

The $c_\perp$ polarized reflection spectrum for (010) is devoid of structure in the energy region corresponding to the CT-I transition. The lowest energy structure occurs at 24 200 cm^{-1} in the dispersion tail due to the S_1 anthracene vibronic transitions. Treatment of the crystal back surface to spoil possible back reflection effects failed to affect either the magnitude or the position of this structure. This weak enhanced reflectivity occurring at 24 200 cm^{-1} in both polarizations provides the first evidence for a non-center-to-center polarization of the CT-II transition.

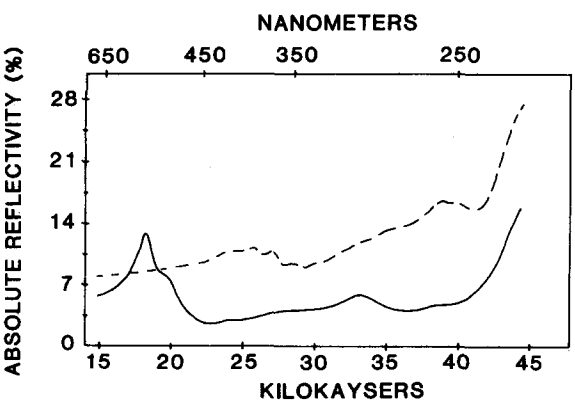

FIG. 5. PMDA–A reflection spectra at 300 K for the c-axis (—) and $c_\perp$-axis (---) directions on (010).

The ~ 1400 cm^{-1} vibronic progression of the S_1 anthracene transition commences at 25 800 cm^{-1} in the $c_\perp$ (010) spectrum. The reflection maximum of 11.29% due to the (0, 0) vibronic transition is red shifted 900 cm^{-1} relative to the corresponding solution absorption band in iso-octane.

The spectral congestion noted in the 30 000–45 000 cm^{-1} region of the $c_\perp$ spectrum is due to both PMDA transitions and the S_2 of anthracene. A local maximum of 16.61% at 39 000 cm^{-1} due predominantly to the anthracene S_2 occurs approximately 1000 cm^{-1} to the red of the corresponding solution absorption band in iso-octane. Whereas the reflection maxima due to the long and short axis polarized anthracene transitions are red shifted approximately 1000 cm^{-1} relative to the corresponding solution absorption bands, the crystal shift of the lowest energy charge transfer transitions is almost three times larger.

The prominent reflection maxima observed in the E polarized spectrum of the (001) face at 32 800 and 37 900 cm^{-1} with corresponding reflectivities of 27.37% and 44.02%, respectively, result from the large projected intensities of the anthracene and PMDA long axis polarized transitions. In the dispersion tail due to the high energy reflection bands, rather diffuse structure at ~ 18 300 and ~ 24 200 cm^{-1} due to CT-I and CT-II, respectively, is observed. The weak reflectivities due to CT-I and CT-II are a consequence of the rather large angle (51.29°) subtended by E and c.

The $E_\perp$ polarized (001) face reflection spectrum is taken along a polarization direction that is virtually coincident with the projections of the PMDA and anthracene short axes. The vibronic progression due to the anthracene S_1 transition is easily recognized and the corresponding reflection peaks coincide in energy with those observed in the $c_\perp$ (010) spectrum. Also present in the $E_\perp$ spectrum are local reflection maxima at 24 200 and 34 900 cm^{-1} due to the CT-II and short axis polarized PMDA transitions.

The 20 K, c-axis (010) face, PMDA–A reflection spectrum is shown in Fig. 7. Although the lowest en-

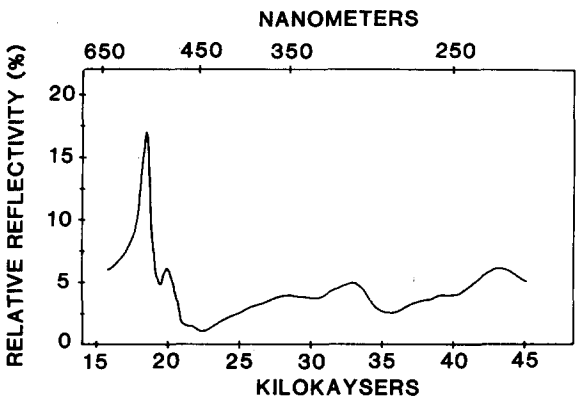

FIG. 7. PMDA–A reflection spectrum at 20 K for the c-axis direction on (010).

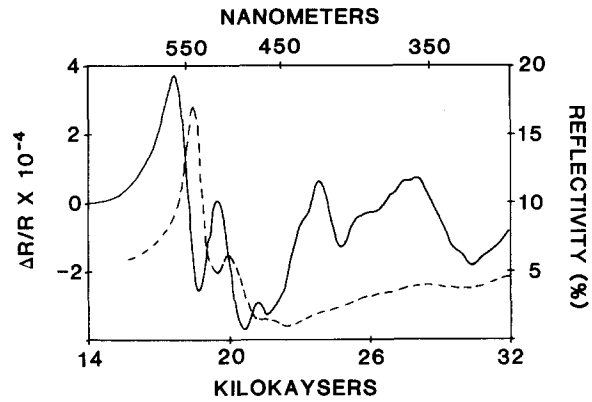

FIG. 9. PMDA–A reflection spectrum at 20 K (---) and piezoreflection spectrum (—) at 300 K for the c-axis direction on (010).

ergy reflection band due to the CT-I transition is resolved into three vibronic components, the reflection structure associated with CT-II and CT-III remains weak and diffuse.

Both the potential strain sensitivity of the CT transitions and the need for increased resolution of the optical response function in the energy region corresponding to CT-II and CT-III prompted the piezospectroscopic examination of PMDA–A. The crystal also serves as a model for the no-coupling regime.

B. Piezoreflection spectra

The acquisition of piezoreflection spectra from the (010) face of PMDA–A was facilitated by the use of the instrumentation procedures described elsewhere.[20] Thin platelets harvested from the growth solution were subsequently bonded to the piezoelectric transducer surface for piezoreflection experiments.

The visible region reflection and piezoreflection spectra for the c axis for the (010) face are shown in Fig. 8. The plot convention for the primary data R and $\Delta R/R$ introduced here will be maintained throughout the remaining sections. All piezospectroscopic quantities represent root mean square values corresponding to a compressive–extensive strain cycle.

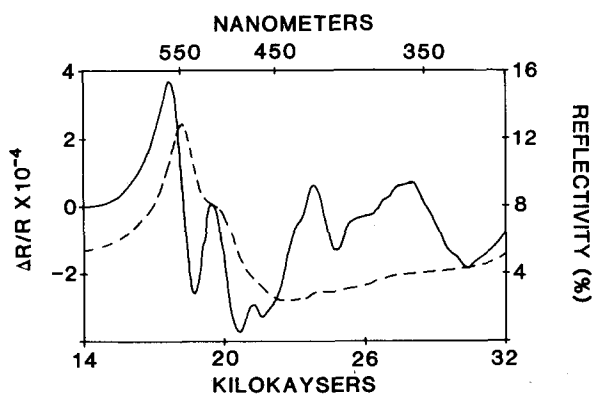

FIG. 8. PMDA–A reflection (---) and piezoreflection (—) spectra at 300 K for the c-axis direction on (010).

The reflection and piezoreflection spectra were recorded with a resolution of 50 cm^{-1}. Despite this, the piezoreflection spectrum exhibits rather dramatic enhancement of structure relative to that realized in the unmodulated reflection spectrum. The low energy reflection band corresponding to CT-I is distinctly resolved into three very prominent derivative-like components which exhibit local maxima at 17 760, 19 530, and 21 280 cm^{-1}. The positive peak value for $\Delta R/R$ of 3.734×10^{-4} occurs at 17 760 cm^{-1} whereas the maximum negative excursion of the piezoreflection signal is -3.750×10^{-4} at 20 660 cm^{-1}.

The two derivative-like excursions in $\Delta R/R$ exhibiting local maxima at 23 920 and 28 010 cm^{-1} approximately locate the two high energy charge transfer transitions CT-II and CT-III, respectively. In contrast to the rather smooth derivative-like $\Delta R/R$ curve in the vicinity of the CT-II transitions, the piezoreflectance profile in the CT-III energy region is quite structured. The small, distinct undulations superimposed on the derivative-like profile in the 25 500 to 31 000 cm^{-1} region are characterized by a periodicity of approximately 1400 cm^{-1}. This demonstrates that the sensitivity of the $\Delta R/R$ spectrum is sufficient to observe the small amount of intensity projected by the anthracene S_1 onto the c axis.

A comparison between the room temperature $\Delta R/R$ spectrum and the 20 K reflection spectrum is shown in Fig. 9. The spectral structure in the CT-I region of the $\Delta R/R$ spectrum is comparable to that in the low temperature reflection spectrum. These are also in agreement with the progressions observed at 2 K.[4] The shoulders observed at 19 000 and 22 000 cm^{-1} also have corresponding structure, allowing for a red shift on cooling, in the 2 K spectra. In the energy range spanned by the CT-II and CT-III transitions, however, the structural enhancement observed in the $\Delta R/R$ spectrum is definitely superior to that of the 20 K spectrum. A comparison of $\Delta R/R$ with the logarithmic energy derivative of R is used for analysis of the piezoreflectance spectrum. Figure 10 shows the superimposed R, $\Delta R/R$, and $(1/R)(dR/d\tilde{\nu})$ spectral profiles in the 14 000 to 32 000 cm^{-1} region for the c principal direction of the (010)

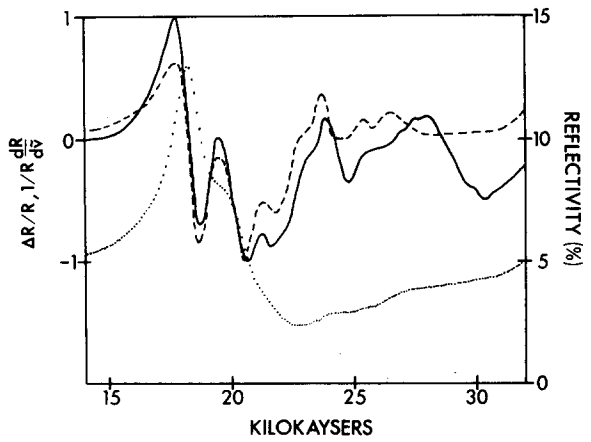

FIG. 10. PMDA-A c-axis reflection (•••) and piezoreflection (—) and calculated logarithmic derivative (---) spectral profiles for (010) at 300 K.

face. The quantity $(1/R)(dR/d\tilde{\nu})$ $[=(1/R)(\Delta R/\Delta\tilde{\nu})]$ represents the logarithmic photon energy derivative which was calculated numerically from the reflection spectrum at 100 cm^{-1} intervals. The $\Delta R/R$ and $(1/R)(dR/d\tilde{\nu})$ curves were normalized by the magnitude of the maximum value in the 14 000–32 000 cm^{-1} region.

The close correspondence between the piezoreflection spectrum and the logarithmic energy derivative shown in Fig. 10 indicates that the strain modulation of the reflection spectrum primarily arises from a perturbation of the crystal transition energies. The coincidence between $\Delta R/R$ and $(1/R)(dR/d\tilde{\nu})$ deteriorates in the energy region corresponding to the CT-II and CT-III transitions. Although the strain sensitivities of the latter may differ from that of the CT-I transition, it should be noted that the quality of the calculated derivative in this energy region is rather poor due to the low crystal reflectivities and diffuse nature of the structure. Taking cognizance of the discussion presented in the previous paper[1] concering a comparison between $\Delta R/R$ and $(1/R)(dR/d\tilde{\nu})$, one notes that both the sense (sign) of the $\Delta R/R$ with respect to $(1/R)(dR/d\tilde{\nu})$ and the comparable relative magnitudes of the excursions which occur in the two profiles over the energy range corresponding to the CT-I vibronic transitions indicate that the latter undergo approximately equal red shifts due to lattice compression. Any disparity between $\Delta R/R$ and $(1/R)(dR/d\tilde{\nu})$ with respect to the relative magnitudes of the structure contained therein is a clear indication of either differences in strain sensitivity among the relevant transitions or nonconformity to a strict transition energy derivative.

The coincidence between the piezoreflection spectrum and the logarithmic energy derivative in the energy region corresponding to the CT-I transition permits numerical calculations of the strain-induced shifts of the vibronic transition energies. These were evaluated for the three prominent vibronic resonances from the unnormalized $\Delta R/R$ and $(1/R)(dR/d\tilde{\nu})$ curves by two comparable methods. The first procedure used to determine a particular vibronic transition energy strain shift entails averaging the two values of the $\Delta R/R$ to

TABLE III. Strain-induced shifts of vibronic transition energies.

	Anthracene	CT–I
Vibronic transition	ΔE (cm^{-1})	ΔE (cm^{-1})
(0, 0)	-0.56 ± 0.05	-0.79 ± 0.1
(0, 1)	-0.58 ± 0.05	-0.82 ± 0.1
(0, 2)	-0.54 ± 0.05	-0.70 ± 0.1
Average	-0.56 ± 0.05	-0.77 ± 0.1

$(1/R)(dR/d\tilde{\nu})$ ratio calculated at the energies corresponding to the peak and troughs of the two profiles. The second method, which yields a slightly more reliable value for strain shift, involves ratioing the change in $\Delta R/R$ measured from peak to trough by the corresponding change in $(1/R)(dR/d\tilde{\nu})$. This procedure diminishes the need for considering the slight background or zero offset signal invariably present in the $\Delta R/R$ spectrum. The differences in the CT-I vibronic transition energy strain shifts calculated by the two procedures were found to be less than 0.1 cm^{-1}.

The strain-induced shifts of the CT-I vibronic transition energies are given in Table III. The shifts correspond to an isotropic, planar compressive strain of 6.3×10^{-5} applied to the (010) face of PMDA–A. The strain-induced changes in the a and c lattice parameters are calculated to be

$$\Delta a \cong -4.61\times10^{-4}\ \text{Å}\ ,$$

$$\Delta c \cong -4.51\times10^{-4}\ \text{Å}\ .$$

Within the estimated uncertainty of the strain shift calculations, there are no detectable differences in the strain shifts of the three vibronic transitions.

C. Anthracene S_1 transition

The superimposed $c_\perp$ polarized reflected and piezoreflection spectra obtained in the 22 000 to 32 000 cm^{-1} energy region from the (010) face are shown in Fig. 11. The piezoreflection spectrum in this region resolves the anthracene vibronic progression into five derivative-like components which exhbit local minima in $\Delta R/R$ at

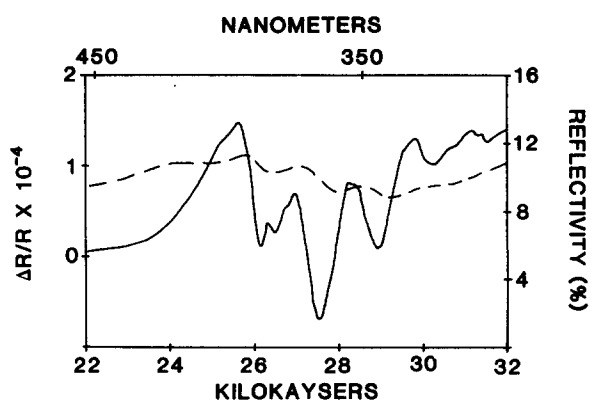

FIG. 11. PMDA–A $c_\perp$-axis reflection (---) and piezoreflection (—) spectra for (010) at 300 K.

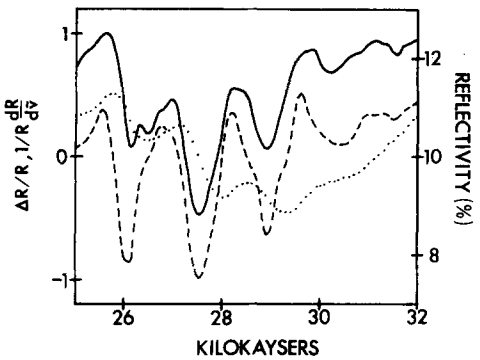

FIG. 12. PMDA-A $c_\perp$-axis reflection (•••), piezoreflection (—), and logarithmic derivative (---) spectral profiles in the region of the anthracene S_1.

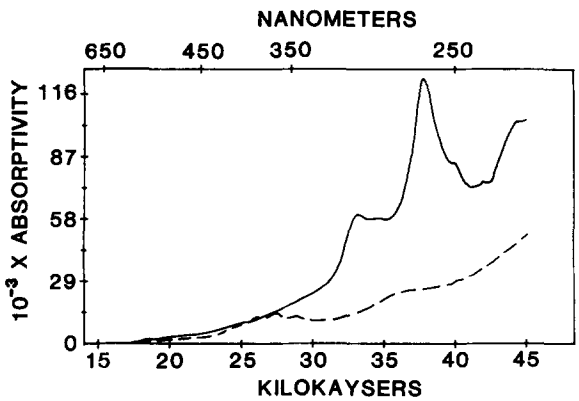

FIG. 14. PMDA–A Kramers-Kronig transformed absorption spectra for (001). **E** (—) and $\mathbf{E}_\perp$ (---).

26 100, 27 530, 28 870, 30 180, and 32 020 cm^{-1}. The maximum positive value attained by $\Delta R/R$ is 1.478×10^{-4} at 25 580 cm^{-1} whereas the extreme negative excursion of the piezoreflection signal is -6.9×10^{-5} at 27 530 cm^{-1}. The structure in the piezoreflection spectrum is sufficient to permit the recognition of weak structure which is completely obscured in the reflection spectrum. Specifically, structure is noted to occur in the vicinity of the (0, 0) vibronic transition at 26 100, 26 460, and 26 810 cm^{-1}. The energy separations of the latter (360 and 350 cm^{-1}) strongly suggest that the vibronic progression due to the totally symmetric 392 cm^{-1} anthracene vibration has been resolved in the $\Delta R/R$ spectrum. The piezoreflectance line shape in the energy region corresponding to the CT-II transition is considerably different from that observed in the same region of the c (010) face $\Delta R/R$ spectrum. This is attributed to interference arising from a disparity in the strain sensitivities of the overlapped CT-II and (0, 0) anthracene vibronic transitions. Figure 12 shows the R, $\Delta R/R$, and $(1/R)(dR/d\tilde{\nu})$ spectral profiles relevant to the $c_\perp$ (010) principal direction in the 25 000 to 32 000 cm^{-1} region.

Both the sense (sign) of $\Delta R/R$ with respect to $(1/R)(dR/d\tilde{\nu})$ and the comparable relative magnitudes of the spectral features observed in the two profiles indicate that the anthracene vibronic transitions undergo approximately equal strain-induced energy shifts to the red due to lattice compression. Furthermore, the close correspondence between $\Delta R/R$ and $(1/R)(dR/d\tilde{\nu})$ obtains even for the rather weak structure present in the 30 000–32 000 cm^{-1} energy region. The strain-induced shifts of the anthracene vibronic transition energies were calculated in a manner previously described for the CT-I vibronic transitions. These shifts are also given in Table III.

A comparison between the average ΔE values obtained for the CT-I and anthracene S_1 vibronic transitions indicates that the strain-induced shift of the former is approximately 0.21 cm^{-1} greater than that of the latter. Although this result is qualitatively explicable in terms of the nature of the two types of excitations, i.e., inter- versus intramolecular, the observed disparity in the modulation sensitivities of the CT-I and anthracene vibronic transitions is somewhat less than that which would be anticipated from a consideration of the observed solution-to-crystal energy shifts experienced by the two transitions.

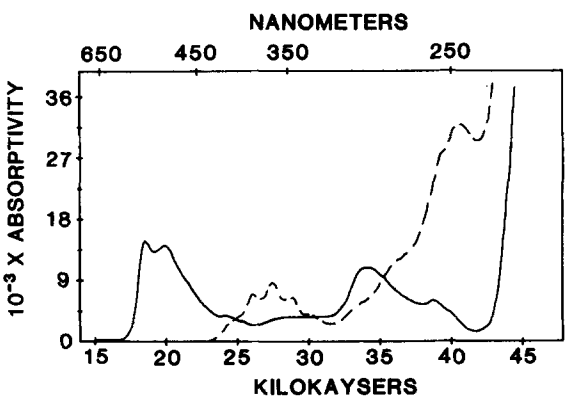

FIG. 13. PMDA–A Kramers-Kronig transformed absorption spectra for (010). c axis (—) and $c_\perp$ axis (---).

D. Absorption and piezoabsorption

1. *Absorption spectra*

The Kramers-Kronig transformed absorption spectra for the (010) and (001) faces of PMDA–A are shown in Figs. 13 and 14, respectively. The (0, 0) and (0, 1) vibronic components of CT-I are observable in the c polarized spectrum of (010) as two prominent absorption maxima occurring at 18 600 and 19 900 cm^{-1}, respectively. A comparison between the (0, 0) transition energy and the energy of the charge transfer transition observed in the solution spectrum shows a -2680 cm^{-1} solution-to-crystal shift of the CT-I excitation. The position of the weak absorption profile due to the latter in the E polarized (001) spectrum indicates that there is no observable directional dispersion of the transition energy. Furthermore, the $c/c_\perp$ polarization ratio for the CT-I transition deduced from the (010) spectra is found to be virtually infinite.

The (0, 0) and (0, 1) vibronic components of the second charge transfer transition CT-II are in evidence at 24 200 and 25 700 cm^{-1}, respectively, in the c (010) face

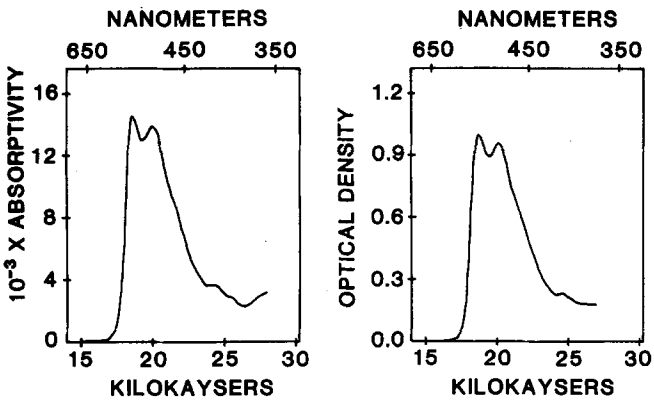

FIG. 15. PMDA–A c-axis Kramers-Kronig transformed absorption spectrum (left) and thin film absorption spectrum (right) from (010).

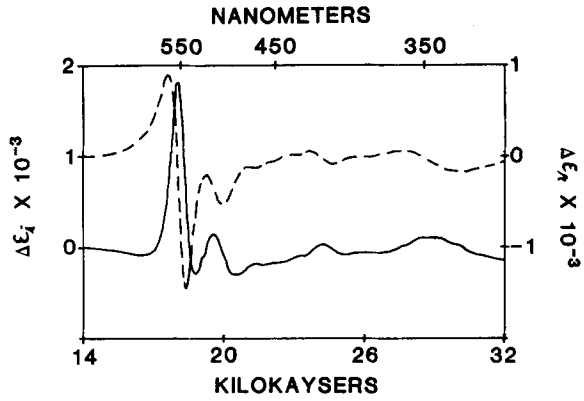

FIG. 17. PMDA–A c-axis Kramers-Kronig ϵ_i (—) and ϵ_r (---) spectra from (010) at 300 K.

spectrum. Weak absorption maxima due to this transition are, within error, observable at the same energy (24 200 cm^{-1}) in all the polarized spectra obtained from the (010) and (001) faces. The $c/c_\perp$ polarization ratio for CT-II is 2.10. This value and the $E/E_\perp$ polarization ratio of 1.76 determined from the (001) face spectra indicate that the CT-II transition moment direction deviates from the PMDA–A complex line of centers.

The somewhat unusual absorption envelope due to the CT-I vibronic transitions has been graphically deconvoluted to yield the following Franck–Condon factors for the five members of the progression: 0.360, 0.321, 0.198, 0.109, and 0.012. The comparable crystal absorptivities due to the CT-I (0, 0) and (0, 1) vibronic transitions observed in the Kramers-Kronig transformed c (010) face spectrum are also observed in the corresponding PMDA–A thin film absorption spectrum shown in Fig. 15. The charge transfer absorption spectrum presented here is in some disagreement with one reported earlier.[21] This may arise from differences in film preparation.

The Kramers-Kronig transformed absorption spectra for both the c and $c_\perp$ principal directions of (010) in the energy region corresponding to the CT-II transition were confirmed by thin film absorption spectroscopy. Figure 16 shows the absorption spectra for the c and $c_\perp$ principal directions. The presence of absorption due to CT-II at ~ 24 200 cm^{-1} for both the c and $c_\perp$ polarization directions establishes the non-center-to-center polarization of the transition.

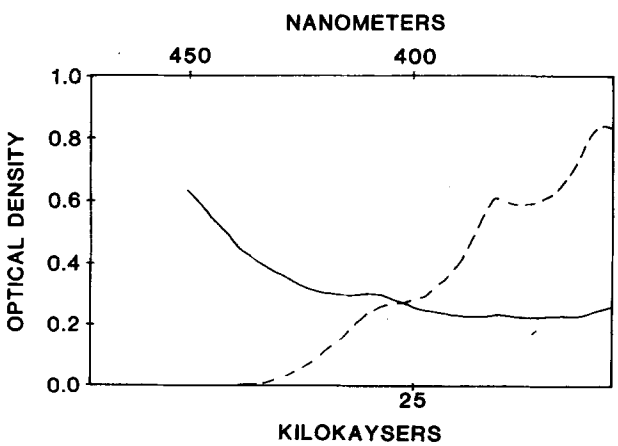

FIG. 16. PMDA–A c-axis (—) and $c_\perp$-axis (---) thin film absorption spectra from (010) in the CT-II region.

The highest energy PMDA–A charge transfer transition CT-III appears as a diffuse, weak, structureless absorption band which has a local maximum at ~ 28 700 cm^{-1} in the c polarized (010) face spectrum. There is also evidence for the existence of this transition in the E (001) spectrum. An unambiguous determination of the $c/c_\perp$ polarization ratio for the CT-III transition is difficult because the absorption profile of the latter spans the approximate energy range of the anthracene S_1 transition. However, the CT-III transition appears to project little or no intensity onto the $c_\perp$ direction wherein an unperturbed intensity progression is observed for the S_1 anthracene vibronic transitions.

The S_1 anthracene transition commences at 26 100 cm^{-1} in both the $c_\perp$ (010) and $E_\perp$ (001) spectra. Interference from PMDA transitions renders the determination of the anthracene S_2 transition energy difficult. The best value for the latter is taken to be 37 800 cm^{-1}, which corresponds to the prominent absorption maximum observed in the E polarized (001) face spectrum.

Although the polarizations of the PMDA molecular transitions are not unambiguously established, maxima due to the latter are clearly observed at 33 300 and 34 700 cm^{-1} in the E (001) face spectrum and 34 200 cm^{-1} in the c (010) face spectrum. The PMDA transition energies observed in the crystal spectra agree reasonably with the absorption maxima observed in the solution spectrum in glacial acetic acid.

2. Differential Kramers-Kronig transforms–piezospectroscopic data

The profiles of the strain-induced changes in the crystal dielectric function for the c principal direction of the (010) face in the 14 000–32 000 cm^{-1} energy region are shown in Fig. 17. The piezospectroscopic data obtained for the c principal direction of (010) in conjunc-

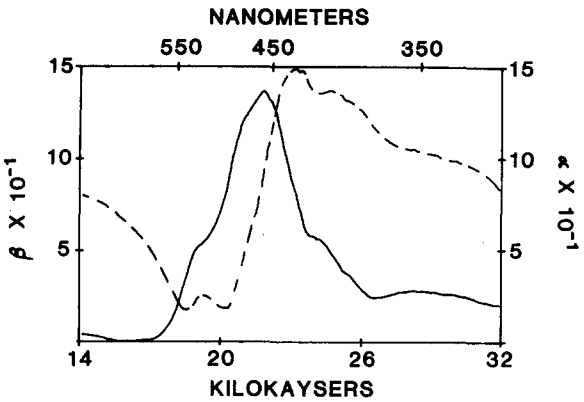

FIG. 18. PMDA–A c-axis Seraphin coefficients for (010). α (---) and β (—).

tion with the frequency dependence of the Seraphin coefficients[1,22] α and β, shown in Fig. 18, permits a phenomenological description of the piezoreflection spectrum. The positive excursion of $\Delta R/R$ (cf. Fig. 8) in the region from 14 000 to 17 800 cm^{-1} is attributed to the $\alpha\Delta\epsilon_r$ product in the expression

$$\Delta R/R = \alpha\Delta\epsilon_r + \beta\Delta\epsilon_i \ .$$

In the energy region corresponding to the absorption maxima due to CT-I vibronic transitions, the weighting factor β is large relative to α and the $\beta\Delta\epsilon_i$ product determines the piezoreflectance line shape from ~ 18 500 to 22 000 cm^{-1}. The maxima and minima in the $\Delta\epsilon_i$ spectrum over this energy range correspond to those for the $\Delta R/R$ spectrum. The derivative-like $\Delta R/R$ structure in the vicinity of the CT-II and CT-III transitions derives primarily from the strain modulation of the real part of the dielectric function $\Delta\epsilon_r$ which has a large weighting coefficient α.

A similar analysis of piezospectroscopic data corresponding to vibronic progressions of the short axis polarized anthracene transition in the 22 000 to 32 000 cm^{-1} region reveals that the $\Delta\epsilon_r$ modulation is responsible for the observed piezoreflection spectrum. The prominent features of the latter are virtually superimposable (within the bandpass) with those for the $\Delta\epsilon_r$ spectrum.

It should be noted that the strain-induced shifts of both the CT-I and anthracene (0, 0) vibronic transition energies were evaluated from the ratio of the change in $\Delta\epsilon_i$ measured from peak to trough in the relevant (0, 0) energy region to the corresponding change in the numerically calculated derivative $d\epsilon_i/d\tilde{\nu}$. The (0, 0) strain-induced shifts calculated by this procedure were found to agree with those obtained from the $\Delta R/R$ and $(1/R)(dR/d\tilde{\nu})$ data. The entire spectral profiles of $d\epsilon_i/d\tilde{\nu}$ for the c and $c_\perp$ principal directions were, however, not calculated.

3. Transition intensities and polarizations

The crystal directional intensities observed for the PMDA–A charge transfer transitions and the S_1 and S_2 anthracene transitions were analyzed in the manner described by Eckhardt and Eckhardt.[23] In addition to the general calculative procedures which apply to both inter- and intramolecular transitions, the directional and absolute crystal intensities (Table IV) of the charge transfer transitions have been corrected for the doubled absorption cross section of the transition in the crystal.[2]

The CT-I transition moment direction coincides with the PMDA–A complex center-to-center vector or c axis. Absolute dipole strengths for the CT-I transition of 0.198 and 0.179 $Å^2$ were determined from the integrated areas of the corresponding absorption bands present in the c (010) and E (001) spectra, respectively. A com-

TABLE IV. Energies and intensities of observed transitions in crystalline PMDA–A.

Transition	Principal direction	(010) Face $\tilde{\nu}$ (kK)	(010) Face d_p^2 ($Å^2$)[a]	(010) Face d^2 ($Å^2$)[b]	(001) Face $\tilde{\nu}$ (kK)	(001) Face d_p^2 ($Å^2$)[a]	(001) Face d^2 ($Å^2$)[b]
Charge transfer bands							
CT-I	$\parallel \hat{c}$	18.60	0.198	0.198	c	c	c
	$\parallel \hat{E}$	c	c	c	18.60	0.070	0.179
CT-II[d]	$\parallel \hat{c}'$	24.20	0.021	0.031	c	c	c
	$\perp \hat{c}'$	24.20	0.010	0.029	c	c	c
CT-III[e]	$\parallel \hat{c}'$	28.70	0.035	0.035	c	c	c
Anthracene bands							
$\hat{M}_A$ ($^1B_{2u} \leftarrow {}^1A_{1g}$)	$\perp \hat{c}'$	26.10	0.179	0.221	c	c	c
	$\perp \hat{E}$	c	c	c	26.10	0.363	0.368
$\hat{L}_A$ ($^1B_{1u} \leftarrow {}^1A_{1g}$)	$\perp \hat{c}'$	38.80	0.630	3.73	c	c	c
	$\parallel \hat{E}$	c	c	c	37.80	2.35	2.59
PMDA[f] bands							

[a]Directional crystal intensity.
[b]Absolute crystal intensity.
[c]Not applicable.
[d]Data from $\parallel \hat{E}$ and $\perp \hat{E}$ of the (001) face are not suitable for intensity measurements.
[e]Assumed center-to-center polarization. See the text.
[f]Parentage of PMDA transitions is uncertain. See the text for explanation.

parison between the mean values of the dipole strength obtained from crystal spectroscopy (0.189 Å^2) and solution studies (0.143 Å^2) reveals that the CT-I transition in the crystal is moderately hyperchromic.

The determination of the CT-II polarization direction was complicated by the existence of two possible transition moment vectors which are consistent with the measured $c/c_\perp$ and $E/E_\perp$ polarization ratios. The squared projections for the two idealized transition moment vectors, designated as $\hat{\mu}_{CT\text{-}III}$ and $\hat{\mu}_{CT\text{-}II2}$, are virtually indistinguishable insofar as the dichroic ratios are concerned, but the differences in the magnitudes of the directional intensities projected by the two moments are sufficient to permit a determination of the most probable polarization direction for the CT-II transition.

The ratios of the CT-II *directional intensity* obtained from the E (001) face spectrum to the corresponding squared projections of $\hat{\mu}_{CT\text{-}II2}$ and $\hat{\mu}_{CT\text{-}III}$ yield absolute intensities of 0.386 and 0.111 Å^2, respectively. These unreasonably large intensities can be rationalized in terms of the uncertainty associated with deconvolution of the CT-II absorption band in the E (001) face spectrum from the rather intense absorption tail due to higher energy PMDA and anthracene transitions. However, even if one takes cognizance of some excess intensity in the CT-II energy region, the dipole strength of 0.386 Å^2 calculated using the $\hat{\mu}_{CT\text{-}II2}$ fector cannot be easily reduced to yield a realistic value for the intensity. In contrast, the dipole strengths of 0.111 Å^2 calculated from the E (001) spectrum and 0.031 Å^2 calculated from the c (010) spectrum using the squared projection of the $\hat{\mu}_{CT\text{-}III}$ vector are both reasonable and may be brought into better agreement by means of a modest reduction of the 0.111 Å^2 value determined from the congested E (001) spectrum. Hence, the $\hat{\mu}_{CT\text{-}III}$ is regarded as the most probable polarization direction for the CT-II transitions.

It is interesting to consider the orientation of $\hat{\mu}_{CT\text{-}III}$ relative to the PMDA–A complex line of centers. The CT-II transition moment polarization, shown by the dashed arrows in Fig. 3, is directed from the inversion center of the PMDA molecule to the C10 carbon atom of anthracene. Closer inspection reveals that this direction is nearly parallel (within 8°) to the vector between the end ring carbon atom of anthracene C2 and the carbonyl oxygen atom O1 of the PMDA molecule. This strongly suggests that the polarization of CT-II is dictated by the distortion of the PMDA molecular conformation wherein a particular anhydride moiety is strongly associated with the anthracene molecule which resides either above or below it in the alternating donor–acceptor stack. The absorption band observed in the c (010) spectrum at ~ 28 700 cm^{-1} is attributed to the highest energy PMDA–A charge transfer transition CT-III. This assignment is consistent with the small c axis projected intensities of the in-plane anthracene and PMDA molecular transitions. The latter are responsible for the congested c (010) absorption spectrum in the 32 000 to 42 000 cm^{-1} energy region. Unfortunately, the spectral data are insufficient to establish either the polarization or intensity of the CT-III transition. However, both the presence of the CT-III absorption band in the c (010) spectrum and the apparent absence of intensity projected onto the $c_\perp$ direction of the (010) face are indicative that the CT-III polarization direction is nearly parallel to the PMDA–A complex line of centers. The CT-III transition dipole strength calculated from the c (010) directional intensity corrected for the small intensity projected by the S_1 is 0.035 Å^2.

The transition dipole strengths of 0.221 and 0.368 Å^2 for the anthracene S_1 were determined from the integrated areas of the corresponding absorption bands observed in $c_\perp$ (010) and $E_\perp$ (001) spectra, respectively. The absolute intensity of 0.368 Å^2 is in excellent agreement with the values obtained by Craig[15] and Lyons and Morris.[24] The 0.221 Å^2 obtained from the $c_\perp$ (010) spectrum reflects loss in measured intensity due to the axial dispersion. The mean value of the dipole strength is 0.295 Å^2.

The absolute intensities of 3.73 and 2.59 Å^2 for the S_2 of anthracene were obtained from the integrated areas of the corresponding absorption bands present in the $c_\perp$ (010) and E (001) spectra, respectively. The mean intensity of 3.16 Å^2 is in reasonably good agreement with the value of 3.49 Å^2 reported by Lyons and Morris.[24] The small value of 2.59 Å^2 is attributed to uncertainty in the deconvolution of the E (001) spectrum.

The PMDA molecular transitions are partially obscured by the intense absorption band due to the anthracene S_2 which occurs in approximately the same energy region. Only the weak absorption band due to a PMDA transition observed at ~ 36 100 cm^{-1} in the $E_\perp$ (010) spectrum is sufficiently isolated to justify a calculation of the corresponding polarization and intensity. The square of the direction cosine of the PMDA short axis with the $E_\perp$ direction is 0.987. This strongly suggests that the absorption at ~ 36 100 cm^{-1} is attributable to a $\hat{M}_P$ polarized transition. A graphical deconvolution of the PMDA transition intensity from the slowly varying background absorption together with the squared projection of 0.987 yields a dipole strength of 0.151 Å^2. The latter is in general agreement with the solution absorption intensity of 0.101 Å^2 determined from the PMDA spectrum in glacial acetic acid.

VI. DISCUSSION OF RESULTS

The mean value of 0.189 Å^2 for the CT-I transition dipole strength obtained from crystal spectroscopy is comparable to the solution absorption intensity of 0.143 Å^2. Despite the absence of any significant intensification of the crystal transition, the solution-to-crystal shift of the excitation energy is anomalously large. Although the direction of the shift may be easily explained, the precise nature of the crystal interactions responsible for its large magnitude remains an open question. Some insight may be obtained from a brief consideration of both inter- and intracomplex electrostatic interactions.

Both the polarization of the CT-I transition and the intimate anthracene–PMDA stacking arrangement along the c axis suggest that the crystal shift is partially attributable to intrastack exciton resonance. The dipole

active CT-I exciton transition involves a coherent or in-phase arrangement of transition moments oriented along the c axis. If the exciting light is c polarized and propagates normal to the (010) plane, the exciton resonance is transverse and there is no macroscopic dipole field associated with the excitation in the crystal. The residual analytic dipole interaction energy may be estimated from a knowledge of the intercomplex distance and the CT-I transition moment strength.

Restricting attention to intrastack exciton coupling, the pair interaction between dipoles oriented along the c axis may be written as

$$V_{12} = -\frac{2\mu^2}{R_{12}^3} = -\frac{2e^2d^2}{R_{12}^3} .$$

Using the CT-I dipole strength of 0.198 Å^2 obtained from the c (010) spectrum and the value of 7.125 Å for R_{12}, the pairwise interaction energy is -127 cm^{-1} and the coupling energy between dipoles separated by $2R_{12}$ is 15.89 cm^{-1}. Summation of these interaction energies and multiplication of the result by two yields a zeroth order exciton resonance energy of -285.77 cm^{-1}. Although this truncated "lattice sum" procedure is admittedly simplistic, it is doubtful that a rigorously calculated exciton interaction energy would deviate from the above value by more than 50–100 cm^{-1}. Consequently, it appears that exciton resonance is too weak to account for the observed solution-to-crystal shift of CT-I.

The differences in dispersion, repulsion, and exchange interactions between the ground and excited states of an isolated, 1:1 $a\pi$–$b\pi$ complex constitute only a small fraction of the charge transfer transition energy.[11] Because of the short range nature of the forces involved, it is improbable that the differences in ground and excited state intercomplex interactions occurring in the crystal are sufficient to produce the observed CT-I shift. Hence, it is useful to investigate the possible solution-to-crystal changes in intracomplex Coulomb e^2/R_{DA} and charge transfer interactions.

Neglecting exciton resonance and the excited–ground state differences in dispersion, repulsion, and exchange interactions, the charge transfer transition energy is given from Eq. (2.1) as

$$E_{CT} \cong \Delta + \frac{\beta_0^2+\beta_1^2}{\Delta} \cong \Delta + \frac{2k^2S_{01}^2}{\Delta} ,$$

where

$$\Delta = I_D - E_A - \frac{e^2}{R_{DA}} ,$$

$$\frac{\beta_0^2}{\Delta} = \frac{k^2S_{01}^2}{\Delta} = \text{charge transfer stabilization energy of the no-bond state } \psi_0 ,$$

$$\frac{\beta_1^2}{\Delta} = \frac{k^2S_{01}^2}{\Delta} = \text{charge transfer destabilization energy of the dative bond state } \psi_1 ,$$

and I_D represents the vertical ionization potential of the donor molecule, E_A corresponds to the electron affinity of the acceptor, and R_{DA} is the distance between the moieties.

For simplicity, the magnitudes of the charge transfer resonance energies of the ground and excited states are assumed to be equal and S_{01} may be expressed as

$$S_{01} = c\, e^{-R_{DA}} ,$$

where c represents some proportionality constant and R_{DA} corresponds to the distance (6.734 a.u.) between the inversion centers of anthracene and PMDA in the crystal.

A simple model calculation of the PMDA–A, CT-I transition energy may be performed by selecting values for k and S_{01} which are representative of those relevant to weak $a\pi$–$b\pi$ charge transfer complexes. Kadhim and Offen[13] suggest that $k \cong 1$–20 eV and Mulliken and Person[11] assign a value of 0.1 to S_{01}. The following are then taken as approximate parameters for PMDA–A:

$$S_{01} = 0.1 ,$$

$$k = 4 \text{ eV} ,$$

$$W_{01} = 0.4 \text{ eV} ,$$

$$\beta_0^2 = \beta_1^2 = 0.16 \text{ eV}^2 .$$

The CT-I transition corresponds to the excitation of an electron from the highest occupied molecular orbital (HOMO) of anthracene to the lowest unoccupied molecular orbital (LUMO) of PMDA. Haarer *et al.*[25] report a value of 11 ± 1 D for the PMDA–A excited state dipole moment. Therefore, approximately one electron is transferred from anthracene to PMDA. Clark *et al.*[26] have determined the vertical ionization energies of anthracene from photoelectron spectroscopy. The three lowest values for I_D and the corresponding orbital designations are (in eV) 7.40 (b_{3g}) 8.52 (b_{2g}), and 9.16 (a_u). The electron affinity of the PMDA molecule E_A is reported by Ishii *et al.*[27] to be $\cong 1.6$ eV.

The Coulomb interaction energy in the point-charge approximation wherein the charges are localized at the centers of anthracene and PMDA molecules is found to be -4.04 eV for $R_{DA} = 3.562$ Å. In lieu of a point-charge calculation, Mulliken and Person[11] have discussed a somewhat more realistic approximation for evaluating the Coulomb interaction energy. The Coulomb energy is determined by distributing the charge equally among the six carbon atoms of the central acceptor (or donor). This spread-charge model yields interaction energies approximately 14%–21% lower than those evaluated using the point-charge method. If one reduces -4.04 eV by 14%–21%, the maximum and minimum values for the spread-charge Coulomb interaction between $A^+ \cdots PMDA^-$ are -3.46 and -3.18 eV, respectively. Consequently, the extreme values for both and E_{CT} corresponding to the CT-I transition of PMDA–A are

$$\Delta = 18\,870 \text{ cm}^{-1} , \quad E_{CT} = 20\,000 \text{ cm}^{-1} \quad (5.6\%)$$

and:

$$\Delta = 21\,130 \text{ cm}^{-1} , \quad E_{CT} = 22\,100 \text{ cm}^{-1} \quad (4.4\%) ,$$

where the percentages given in parentheses represent contributions to E_{CT} due to the charge transfer interactions between ψ_0 and ψ_1. The calculated values of E_{CT} are in good agreement with those obtained from solution

(21 280 cm^{-1}) and crystal spectroscopy (18 600 cm^{-1}). Furthermore, the charge transfer resonance energies $\beta_0^2/\Delta \cong \beta_1^2/\Delta$ are found to be 0.069 eV, which represents a fairly realistic value for the charge transfer stabilization energy of a weak $a\pi$–$b\pi$ complex.[11] The $-\beta_0^2/\Delta$ term makes a small contribution to the binding energy of a crystalline complex which is largely determined by van der Waals, quadrupole–quadrupole, etc. interactions.

The possible relationship between the $A^+ \cdots PMDA^-$ Coulomb interactions in the crystal and the large solution-to-crystal shift of the CT-I transition energy can be examined. Evaluation of the interaction energy using the PMDA–A interplanar separation of 3.332 Å may be more reasonable since the crystal structure data[6] clearly indicate that several PMDA–A atom–atom contact distances are smaller than 3.3 Å. Hence, the solution-to-crystal change in the mean distance between the anthracene and PMDA moieties of the complex may be sufficient to produce the observed shift. A decrease in R_{DA} of 0.1 Å results in a -940 cm^{-1} change in the $PMDA^- \cdots A^+$ Coulomb interaction. These arguments are similar to those for the influence of internal pressures in liquids and solids on the charge transfer transition energies of weak complexes.[28] Rigorous electrostatic and charge transfer interaction calculations will be necessary to unambiguously establish the origin of the CT-I shift.

The difference in energy between the CT-I and CT-III transitions is noted to be approximately 10 100 cm^{-1}. Qualification is necessary because the diffuse nature of the CT-III absorption band observed in the **c** (010) spectrum precludes an accurate determination of the transition energy. However, the energy separation between the two charge transfer transitions is sufficiently close to the difference in the first and second ionization potentials of anthracene (9034 cm^{-1}) to argue that the CT-III transition involves the excitation of an electron from the penultimately filled anthracene orbital to the LUMO of PMDA. Higher CT transitions with similar energy splittings from the lowest CT band have been observed in the trinitrobenzene–anthracene complex.[23]

The origin of the CT-II transition is more difficult to assign. A recent *ab initio* calculation[29] on the molecule has shown that, as the symmetry constraints on the calculation of PMDA are lowered from D_{2h} to C_s, the lowest energy $\pi^* - n$ singlet energy decreases while the two lowest $\pi^* - \pi$ singlets change only slightly. Since the same π^* orbital is common to all of these transitions, it is clear that the nonbonding orbital involved is extremely sensitive to the symmetry. These results permit reasonable estimate of the transitions in PMDA–A. The calculated $\pi^* - n$ energy is ~ 3.20 eV for the C_s symmetry constraint. The free PMDA–A CT transition energy is 2.64 eV. This latter value permits proper relative registration of the PMDA and A orbitals on the same energy scale. The S_1 of anthracene allows location of the LUMO of anthracene relative to the LUMO of PMDA. The former is ~ 0.7 eV above the latter. With this arrangement, the calculated CT transition arising from a back donation of the PMDA nonbonding orbital to the LUMO of anthracene is ~ 3.9 eV, which, however, is greater than that observed. The CT transition from the HOMO of anthracene to the LUMO of PMDA would be at 3.8 eV. However, the energies of the various states involved are only approximate and could easily be a few tenths of a volt in error. In fact, were the $\pi^* - n$ in PMDA for the geometry in the crystal observed at 3.0 eV, the crystal spectrum would be in agreement with this analysis. The calculation also emphasizes that under the C_s symmetry constraint, the nonbonding orbital is highly localized on the carbonyl oxygens. This would be expected to lead to a CT transition polarized between the carbonyl and the anthracene. The evidence cited supports an assignment of the CT-II transition as a back donation from the occupied nonbonding HOMO of PMDA to the LUMO of anthracene.

The strain-induced shift of the CT-I transition energy can be evaluated using the parameters employed in the previously given model calculation for E_{CT}:

$$dE_{CT} \cong d\Delta + \frac{4k^2 S_{01}}{\Delta} dS_{01} - \frac{2k^2 S_{01}^2}{(\Delta)^2} d\Delta \ ,$$

$$dE_{CT} \cong d\Delta - \frac{4k^2 S_{01}^2}{\Delta} dR_{DA} - \frac{2k^2 S_{01}^2}{(\Delta)^2} d\Delta \ ,$$

where

$$dS_{01} = -S_{01} dR_{DA} \ ,$$

$$dR_{DA} = -4.25 \times 10^{-4} \text{ a.u.} \ .$$

The magnitude of dR_{DA} is calculated from the experimental value of the strain and the lattice parameters. Using the parameters relevant to the calculated value of 20 000 cm^{-1} for E_{CT}, the compressional strain-induced shift of the transition energy is $dE_{CT} = -0.73$ cm^{-1}. The latter represents the sum of strain-induced red and blue shifts of -1.77 and 1.04 cm^{-1}, respectively. The mean value for the strain-induced shift of the CT-I transition energy determined experimentally is -0.77 cm^{-1}. The agreement between the calculated and experimental values for both E_{CT} and dE_{CT} is very good. Undoubtedly, this is somewhat fortuitous. This is particularly true concerning the calculations of dE_{CT} wherein the blue shift of 1.04 cm^{-1} due to the effect of strain on the charge transfer interactions depends on the previously assumed magnitudes for k and S_{01}. However, in this regard, even small values for the latter result in a substantial blue shift of the charge transfer transition energy which reduces the red shift arising from the large difference in Coulomb interactions between the ground and excited states. The most significant aspect of these simple model calculations for E_{CT} and dE_{CT} is the fact that, whereas the charge transfer resonance between ψ_0 and ψ_1 contributes only 5.6% to E_{CT}, the strain differential of such interactions constitutes 37% of dE_{CT}. This is a consequence of the fact that the charge transfer stabilization energies are quadratic functions of S_{01} which, in turn, is an exponential of R_{DA}. Therefore, it appears that the comparable magnitudes observed for the mean strain shifts of the CT-I and anthracene S_1 transitions (-0.77 and -0.56 cm^{-1}, respectively) may be explicable in terms of a significant reduction in the strain-induced red shift of E_{CT}

due to the opposing blue shift contribution arising from the modulation of charge transfer interactions.

The measured CT-I strain shift (-0.77 cm^{-1}) corresponds to a difference in ground and excited state deformation potentials of -3400 cm^{-1}/Å which is comparable to an estimated value of -10000 cm^{-1}/Å reported by both Prochorow and Tramer[30] and Czekalla *et al.*[31] A naive comparison between the magnitude of the CT-I strain shift determined from piezoreflection experiments and a typical shift for a weak complex obtained from high pressure optical spectroscopy studies can be made. Although the elastic constants of PMDA–A are unknown, it may be assumed that they are comparable to those of the trinitrobenzene–anthracene (TNB–A) complex. Dano *et al.*[32] reported a Young's modulus for the stacking direction in TNB–A of 1.25×10^{11} dyn/cm^2. Using this value for the **c** direction in PMDA–A and the experimental strain of 6.33×10^{-5} yields an equivalent pressure of 7.85 bar. Hence, the pressure shift of the CT-I transition found by piezomodulation spectroscopy is found to be approximately -98 cm^{-1}/kbar, which is comparable to the value of -50.4/kbar measured by Kadhim and Offen[13] for the lowest energy charge transfer transition of the crystalline TNB–A complex. The CT-I pressure shift reported herein is comparable to those for the lower members of the polyacene series.[33]

VII. CONCLUSIONS

Comparisons between the $\Delta R/R$ and $(1/R)(dR/d\bar{\nu})$ spectral profiles corresponding to both the charge transfer and anthracene S_1 transitions reveal that the principal effect of lattice strain is a perturbation of the crystal excitation energies. Furthermore, the elucidation of weak spectral features is considerably better in the differential optical response functions $\Delta R/R$ and $\Delta\epsilon_i$ than in the unmodulated data. Hence, a very favorable experimental signal-to-noise ratio is attained at room temperature and relatively low monochromator resolution. The piezomodulation data also permit the determination of the difference in deformation potentials of the ground and lowest energy charge transfer state in PMDA–A. The latter appears to indicate that charge transfer interactions are quite important in determining the magnitude of the piezoreflection signal. In this regard, it would be interesting to investigate a series of complexes exhibiting a wide range of charge transfer interactions.

The oriented gas approximation has been shown to hold particularly well for the intramolecular transitions in crystals of weak pi complexes. In the case of TNB–A and PMDA–A the coupling of the first CT transitions has been shown to be very weak.[2,4] The piezomodulation spectra $\Delta R/R$ in this case follow the calculated derivative $(1/R)(dR/d\bar{\nu})$ of the reflection spectra for the inter- and intramolecular transitions. Such would be expected from crystals with negligible coupling. The fact that the measured derivative is of higher quality than the calculated one is well established.[34]

Thus, the piezomodulation spectra can be used to obtain strain shifts and deformation potentials in the elastic limit for molecular crystals. They are also a sensitive probe for spectroscopic structure. Further, it is suggestive that the extent of agreement of the experimental line shape of the piezoreflection spectrum with the line shape of $(1/R)(dR/d\bar{\nu})$ obtained from the direct reflection spectrum may provide a useful probe to the nature of the coupling in molecular crystals.

[1] J. Merski and C. J. Eckhardt, J. Chem. Phys. 75, 3691 (1981).
[2] C. J. Eckhardt and R. R. Pennelly, J. Am. Chem. Soc. 98, 2034 (1976); C. J. Eckhardt and R. J. Hood, J. Am. Chem. Soc. 101, 6170 (1979).
[3] D. Haarer, Chem. Phys. Lett. 27, 91 (1974).
[4] A. Brillante and M. R. Philpott, J. Chem. Phys. 72, 4019 (1980).
[5] J. C. A. Boeyens and F. H. Herbstein, J. Phys. Chem. 69, 2160 (1965).
[6] B. E. Robertson and J. Stezowski, Acta Crystallogr. Sect. B 34, 3005 (1978).
[7] L. L. Ferstandig, W. G. Toland, and C. D. Heaton, J. Am. Chem. Soc. 83, 1151 (1961).
[8] H. A. Benesi and J. H. Hildebrand, J. Am. Chem. Soc. 71, 2703 (1949).
[9] H. G. Drickamer and C. W. Frank, *Electronic Transitions and the High Pressure Chemistry and Physics of Solids* (Chapman and Hall, London, 1973).
[10] H. W. Offen and T. T. Nakashima, J. Chem. Phys. 47, 4446 (1967).
[11] R. S. Mulliken and W. B. Person, *Molecular Complexes* (Wiley-Interscience, New York, 1969).
[12] R. S. Mulliken, J. Am. Chem. Soc. 64, 811 (1952).
[13] A. H. Kadhim and H. W. Offen, J. Chem. Phys. 48, 749 (1968).
[14] A. Bree and S. Katagiri, J. Mol. Spectrosc. 17, 24 (1965); A. Bree, S. Katagiri, and S. R. Stuart, J. Chem. Phys. 44, 1788 (1966).
[15] D. P. Craig, J. Chem. Soc. 1955, 2302.
[16] J. N. Murrell, *The Theory of the Electronic Spectra of Organic Molecules* (Wiley, New York, 1963).
[17] R. Foster, *Organic Charge-Transfer Complexes* (Academic, New York, 1969).
[18] R. Foster, D. L. Hammick, and A. A. Wardley, J. Chem. Soc. 1953, 3817.
[19] R. L. Scott, Recl. Trav. Chim. Pays-Bas Belg. 75, 787 (1956).
[20] C. J. Eckhardt and J. Merski, Surf. Sci. 37, 937 (1973).
[21] D. Haarer and N. Karl, Chem. Phys. Lett. 21, 49 (1973).
[22] B. O. Seraphin, in *Optical Properties of Solids*, edited by F. Abeles (North-Holland, Amsterdam, 1972).
[23] C. J. Eckhardt and H. Eckhardt, J. Am. Chem. Soc. 102, 2887 (1980).
[24] L. E. Lyons and G. C. Morris, J. Chem. Soc. 1959, 1551.
[25] D. Haarer, M. R. Philpott, and H. Morawitz, J. Chem. Phys. 63, 5238 (1975).
[26] P. A. Clark, F. Brogli, and E. Heilbronner, Helv. Chim. Acta 55, 1415 (1972).
[27] K. Ishii, K. Sakamoto, K. Seki, N. Sato, and H. Inokuchi, Chem. Phys. Lett. 41, 154 (1976).
[28] P. J. Trotter, J. Am. Chem. Soc. 88, 5721 (1966).
[29] C. P. Keijzers, P. S. Bagus, and J. P. Worth, J. Chem. Phys. 69, 4032 (1978).
[30] J. Prochorow and A. Tramer, J. Chem. Phys. 44, 4545 (1966).
[31] J. Czekalla, G. Briegleb, W. Herre, and R. Glier, Z. Elektrochem. 61, 537 (1957).
[32] T. Danno, T. Kajiwara, and H. Inokuchi, Bull. Chem. Soc. Jpn. 40, 2793 (1967).
[33] B. Y. Okamoto and H. G. Drickamer, J. Chem. Phys. 61, 2870 (1974); S. Weiderhom and H. G. Drickamer, J. Phys. Chem. Solids 9, 330 (1959).
[34] I. Shirotani, Y. Kamura, and H. Inokuchi, Mol. Cryst. Liq. Cryst. 28, 345 (1974).